Rare Metal Materials and Engineering
Volume 50, Issue 10, October 2021
Available online at www.rmme.ac.cn

Science Press

Cite this article as: Yang Yaqian, Xing Weiwei, Chen Weiliang, et al. Existence Form and Distribution of Mn and the Effect of Mn Content on High-Temperature Stress Rupture Properties of K417G Superalloy[J]. Rare Metal Materials and Engineering, 2021, 50(10): 3470-3476.

ARTICLE

Existence Form and Distribution of Mn and the Effect of Mn Content on High-Temperature Stress Rupture Properties of K417G Superalloy

Yang Yaqian[1], Xing Weiwei[1], Chen Weiliang[2], Chen Bo[1], Ma Yingche[1], Liu Kui[1]

[1] Shi-changxu Innovation Center for Advanced Materials, Institute of Metal Research, Chinese Academy of Sciences, Shenyang 110016, China; [2] Northeastern University, Shenyang 110819, China

Abstract: The high-temperature stress rupture properties of K417G superalloy with various Mn contents (0.09wt%~0.35wt%) were studied and the existence form and distribution of Mn were evaluated as well. The results show that Mn is solid-dissolved in γ matrix and enriched in γ'-depleted matrix in front of $\gamma+\gamma'$ eutectic cap. Mn elements promote the segregation of Al and Ti to interdendrite zone, thus increasing the volume fraction of $\gamma+\gamma'$ eutectic in interdendrite zone and decreasing the size of γ' phase in dendrite core. With the increase of Mn content, the stress rupture life and the plasticity decrease greatly under the condition of 950 °C/235 MPa. The alloy with the minimal Mn content shows the optimal high-temperature stress rupture properties.

Key words: Mn content; microsegregation; stress rupture properties; existence form; K417G

Nickel-based cast superalloys are widely used in aero-engine turbine blades due to their good performance at elevated temperatures and low manufacturing cost[1-3]. K417G alloy evolved from K417 (IN100) alloy contains amounts of alloying elements, such as Ti, Al, Co and Cr, and is one of the most commonly used materials for typical hot end components of aero-engine. Although the alloy possesses excellent yield and tensile strength, favorable microstructure stability at elevated temperature, the yield and performance stability of castings are low. This is mainly due to the formation of cast porosity and harmful phases during the solidification. Even though effort has been made to refine more stable phases, the formation mechanism of cast porosity and harmful phases is still unknown and needs to be further explored.

Prior studies have shown that Mn tends to segregate around the grain boundaries, weakening the grain boundary binding force and significantly reducing the creep rupture strength of the alloy[4]. In CrNi80Ti alloy, when the Mn content increases from 0.3wt% to 2.5wt%, the stress rupture life decreases by 50%[5]. Besides the detrimental effect of Mn to the grain boundary, the enrichment of such impurity at grain boundaries may also promote the precipitation of harmful phases, which degrades the mechanical properties of the alloy. For instance, in 25Ni-15Cr iron-based superalloy, the fraction of Laves phases increases with the increase of Mn content, which deteriorates the hot workability of the alloy[6]. Mn also has some positive effects, for instance, it can be a getter of S by forming MnS to reduce the detrimental effect of S. In Hastelloy X and Inconel 718 alloys, Mn segregates in the weld fusion zone to decrease the tendency of hot cracking, and improve the weldability[7-9]. In Ni-20Cr alloy, it is found that with the addition of 3wt% Mn, the oxidation resistance can be significantly improved[10].

Mn in K417G alloy is introduced from the raw material during the smelting process. However, the effect of Mn on the microstructure and mechanical properties of K417G is still unknown. The existence form and distribution of Mn in K417G also need to be further explored. Therefore, in this work, the effect of Mn content on high-temperature stress rupture properties and segregation behavior of Mn in K417G were systematically studied, which can provide the experimental evidence and theoretical basis for the optimization of Mn content and further reveal the influence mechanism of Mn in casting superalloy.

Received date: October 20, 2020
Corresponding author: Chen Bo, Ph. D., Professor, Division of Materials for Special Environment, Institute of Metal Research, Chinese Academy of Sciences, Shenyang 110016, P. R. China, Tel: 0086-24-23971986, E-mail: bchen@imr.ac.cn

1 Experiment

In the present work 50 kg master alloy was prepared by vacuum induction melting (VIM) furnace in a CaO crucible. The chemical composition (wt%) of the master ingot was: 9.07 Cr, 10.15 Co, 3.03 Mo, 5.16 Al, 4.44 Ti, 0.78 V, 0.017 B, 0.02 Zr, 0.17 C, 0.0005 O, 0.0003 S, 0.0004 N and the balance Ni. Then it was divided into three parts, re-melted with addition of various amounts of high-purity manganese metal and poured into Al_2O_3 precise shell at the same pouring temperature (1420 °C). Mn content of the round bars was chemically analyzed by inductively couple plasma atomic emission spectrometer (ICP-AES) as 0.09wt% (no addition, residual Mn in master ingot), 0.17wt% and 0.35wt%, named as Mn0.09, Mn0.17 and Mn0.35, respectively.

The round bars for stress rupture test were machined into gauge of ϕ5 mm×25 mm, which was performed at 950 °C with 235 MPa[11] on RJ-30D test machine. The microstructures of different samples were analyzed using Zeiss observer Z1m optical microscope (OM), JEOL JXA-8530F electron probe microanalyzer (EPMA), JSM-6301F scanning electron microscope (SEM) and FEI Tecnai G^2 F30 transmission electron microscope (TEM) equipped with an energy-dispersive X-ray detector. Chemical etching was performed with a solution containing 20 g $CuSO_4$+100 mL HCl+100 mL H_2O+5 mL H_2SO_4, for the general microstructural observation. Deep etching with an electrolyte of 10 mL H_3PO_4 and 90 mL H_2O, which removes γ matrix, was employed for the observation of $\gamma+\gamma'$ eutectic and γ' phase. Sisc IAS image analysis system was used to analyze size and volume fraction of $\gamma+\gamma'$ eutectic and γ' phase. In each specimen, the volume fraction of $\gamma+\gamma'$ eutectic and γ' phase were measured in 20 and 15 different random regions, respectively, to obtain the average value of the microstructure analysis.

2 Results and Discussion

2.1 Microsegregation

Cast samples with various Mn contents were sectioned transversely, ground and polished to characterize the element segregation. The chemical compositions in the dendritic and interdendritic regions were determined by EPMA. The values of elemental segregation coefficient (k) were defined as the ratio of average concentration of alloying elements in the dendrite core to that in the interdendritic region, i. e., $k=C_d/C_i$[12,13]. The value of k less than 1 indicates that the elements tend to segregate to the interdendritic region, while k greater than 1 indicates that the elements are prone to segregate to the dendrite core[14]. As shown in Fig.1, Ti and Al are positivly segregated elements, which tend to concentrate in the residual liquid during solidification corresponding to the interdendritic region in cast. It is noted that the segregation of Ti and Al becomes much more obvious with the increase of Mn content. Cr, Co, V and Mo were negativly segregated elements. The k values of V remain basically unchanged, while the k values of Cr, Co and Mo increase with increasing the Mn content. Mn can be considered as a neutral element, because it has no obvious segregation tendency. But Mn is slightly segregated to the dendrite core with increasing the Mn content.

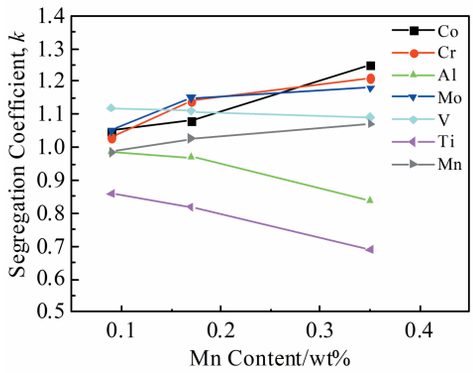

Fig.1 Segregation coefficient k of different elements in the specimens with different Mn contents

2.2 Existence form and distribution of Mn

In order to explore the existing form and distribution of Mn in K417G alloy, three samples with different Mn contents were analyzed by EPMA and TEM. However, with the exception of the common phases which are γ matrix, γ' strengthening phase (Ni_3Al), $\gamma+\gamma'$ eutectic and MC carbides in the as-cast K417G alloy[15], new Mn-rich phase cannot be found. By EDS analysis of TEM, as illustrated in Fig. 2, it is found that the elements of Cr, Co, Mo and Mn are segregated in γ matrix. In other words, Mn is solid-dissolved in the γ matrix.

The result is also confirmed by the first-principles calculation. According to the theoretical research, the substitution enthalpy of Mn for Ni and Ni_3Al is listed in Table 1. All the energy was calculated within the Vienna Ab Initio Simulation Package (VASP) [16,17] with the projector augmented wave (PAW) method[18,19] and generalized gradient approximation described by the parameterization of Perdew-Burke-Ernzerhof function (GGA-PBE) [20]. The computations were performed within a 108-atom periodic supercell. The substitution enthalpy of Mn for Ni_3Al is much higher than that for Ni, in good agreement with the results of Chao et al[21,22]. The results give a positive support for the previous experiments. Therefore, compared to γ' phase, Mn is more likely to dissolve in γ matrix.

According to elemental mapping images obtained through EPMA of Mn0.09 and Mn0.17, Mn is slightly enriched in the γ'-depleted area which is in front of $\gamma+\gamma'$ eutectic, as marked by white lines in Fig.3. At the same time, quantitative analysis was conducted in the γ'-depleted area and the results are listed in Table 2. With increasing the Mn content in the samples, the enrichment of Mn in the γ'-depleted area is more significant. Meanwhile, the content of Cr and Mo in the γ'-depleted area also increases a little with increasing the Mn content, but the content of γ' formation element Al decreases.

$\gamma+\gamma'$ eutectic is formed from the interdendritic residual liquid phase by L→$\gamma+\gamma'$ eutectic reaction during solidification.

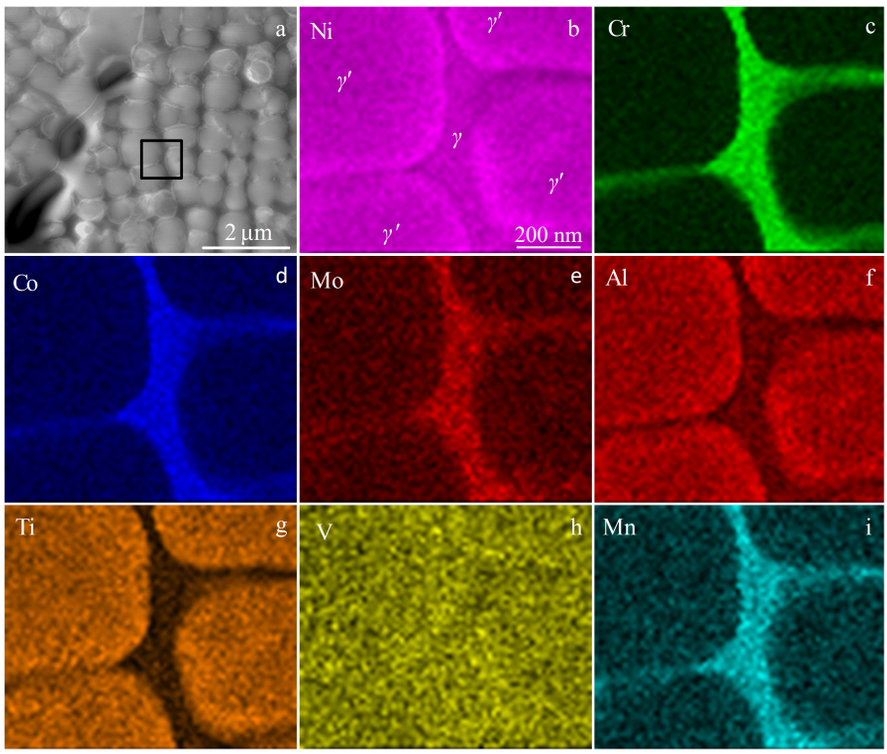

Fig.2 TEM dark-field image of the morphology of γ and γ' in Mn0.35 (a) and corresponding EDS mapping results (b~i)

Table 1 Substitution enthalpy of Mn with Ni and Ni_3Al

Substitution site of Mn	Ni (X_{Ni})	Ni_3Al (X_{Ni})	Ni_3Al (X_{Al})
Substitution enthalpy/eV	-0.43	0.18	1.81

The typical $\gamma+\gamma'$ eutectic is composed of eutectic nucleation zone, eutectic heart and eutectic cap[23], as shown in Fig. 3b. The lamella distance of $\gamma+\gamma'$ eutectic in eutectic heart is very small but at the eutectic cap the distance is very large with massive γ' phase. During solidification, $\gamma+\gamma'$ eutectic is formed in the final stage and the formation consumes little Cr, Co, Mo, Mn elements and more Al, Ti elements compared with the surrounding γ matrix. The reductant Cr, Co, Mo and Mn

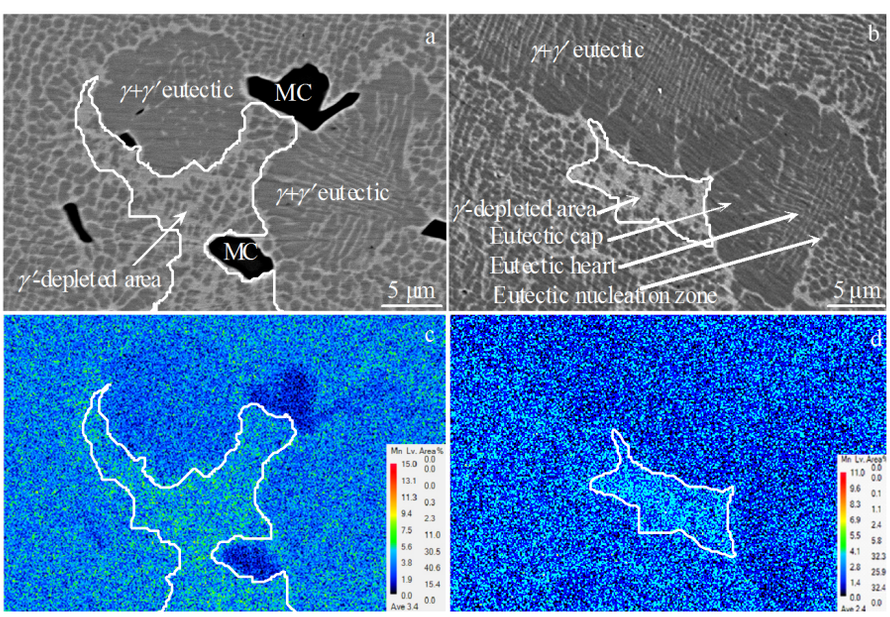

Fig.3 Distribution of Mn element in K417G alloys with different Mn contents: (a, c) Mn0.09 and (b, d) Mn0.17

Table 2 Element content of the matrix in the γ'-depleted area (wt%)

Sample	Co	Cr	Mo	Ti	Al	V	Mn	Ni
Mn0.09	14.180	167.016	3.833	2.567	2.101	0.569	0.204	Bal.
Mn0.17	13.878	16.305	3.977	2.598	2.043	0.551	0.318	Bal.
Mn0.35	14.000	16.791	4.099	2.532	1.905	0.546	0.507	Bal.

elements are expelled to the front of the eutectic cap, resulting in a lower Al, Ti content and a higher Cr, Co, Mo, Mn content in front of the eutectic cap.

2.3 Microstructure evaluation

After etching, the microstructure features of cast samples with various Mn contents were analyzed by OM. As shown in Fig. 4, K417G has a typical dendritic morphology with small amounts of carbides, $\gamma+\gamma'$ eutectic and cast micro-porosity in interdendrite region. The secondary dendrite arm spacing (λ) is an important characteristic parameter of the solidified dendritic structure which directly affects the micro-porosity, element segregation and second phase precipitation[24]. The smaller the secondary dendrite spacing, the smaller the alloy composition segregation, which is conducive to improving the material properties[24,25]. From quantitative calculation listed in Table 3, the secondary dendrite arm spacing of the three specimens is 27.1, 27.7 and 28.3 μm. It can be seen that the addition of Mn element makes the secondary dendrite slightly coarser in K417G superalloy. After calculation, the volume fraction of cast porosity and MC carbide is 0.11%~0.13% and 1.5%~1.7%, respectively. In addition, the Mn content has no significant effect on the morphology and size of MC carbide in K417G superalloy.

Usually, $\gamma+\gamma'$ eutectic is considered as a harmful solidification structure in superalloy. The volume and morphology of $\gamma+\gamma'$ eutectic depend on the chemical composition and cooling rate during solidification[26,27]. By electrolytic corrosion with 10% phosphoric acid solution, the morphology and distribution of $\gamma+\gamma'$ eutectic can be observed very intuitively. As shown in Fig. 5, $\gamma+\gamma'$ eutectic is located in the interdendrite and always can be easily detected around micro-porosities. With the increase of Mn content from 0.09wt% to 0.35wt%, the size of $\gamma+\gamma'$ eutectic is almost the same, but its volume fraction increases from 3.4% to 3.9%, increased by about 14.7%, as shown in Table 3. The formation of the $\gamma+\gamma'$ eutectic is strongly related to the microsegregation. The increased Mn content promotes the segregation of Al and Ti elements into the interdendritic region, and these two elements are the forming elements of the $\gamma+\gamma'$ eutectic. Therefore, more $\gamma+\gamma'$ eutectic is formed.

The γ' phase is the main strengthening phase of precipitation hardened nickel-base superalloys, and its volume fraction, particle size and shape are the decisive factors to the room temperature and high temperature strength of γ'-strengthened superalloys[28,29]. As shown in Fig. 6, γ' particles are in good cubic shape in the dendritic regions with different Mn contents. The volume fraction of γ' phases in the dendrite cores is 63.1%, 62.9% and 63.3%, and the average sizes vary from 642 nm to 579 nm, as listed in Table 3. With increasing the Mn content, the average volume fractions of γ' phases in the dendrite are invariant, but the sizes decrease. As known, Al and Ti elements are also the forming elements of γ' phases. The increased Mn content promotes the segregation of Al and Ti elements into the interdendritic region. Therefore, the content of Al and Ti elements in the dendrite core in Mn0.09 sample is higher than that in Mn0.35 sample, which results in a larger size of γ' phases in Mn0.09 sample.

2.4 Effects of Mn content on the high-temperature stress rupture properties

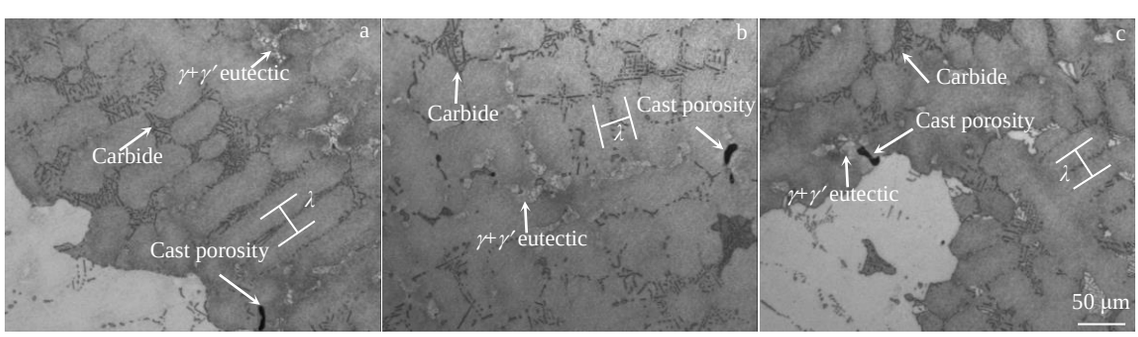

Fig.4 Microstructures and secondary dendrite arm spacing λ of samples with different Mn contents: (a) Mn0.09, (b) Mn0.17 and (c) Mn0.35

Table 3 Microstructure features of cast specimens with different Mn contents

Mn content/wt%	λ/μm	Size of $\gamma+\gamma'$ eutectic/μm	Volume fraction of $\gamma+\gamma'$ eutectic/%	Size of γ' at dendritic core/nm	Volume fraction of γ' phase/%
0.09	27.1±3.6	10.7±0.5	3.4±0.9	642±37	63.1±1.7
0.17	27.7±2.3	11.3±0.5	3.6±0.7	598±55	62.9±2.5
0.35	28.3±2.1	10.8±0.6	3.9±0.8	579±42	63.3±1.0

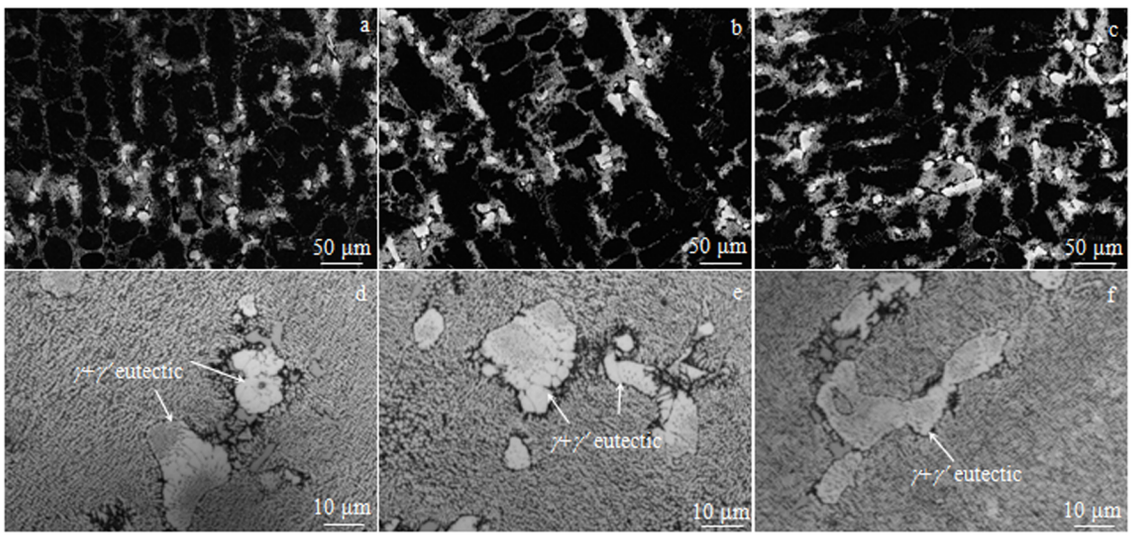

Fig.5 Morphologies and distribution of $\gamma+\gamma'$ eutectic of samples with different Mn contents: (a, d) Mn0.09, (b, e) Mn0.17, and (c, f) Mn0.35

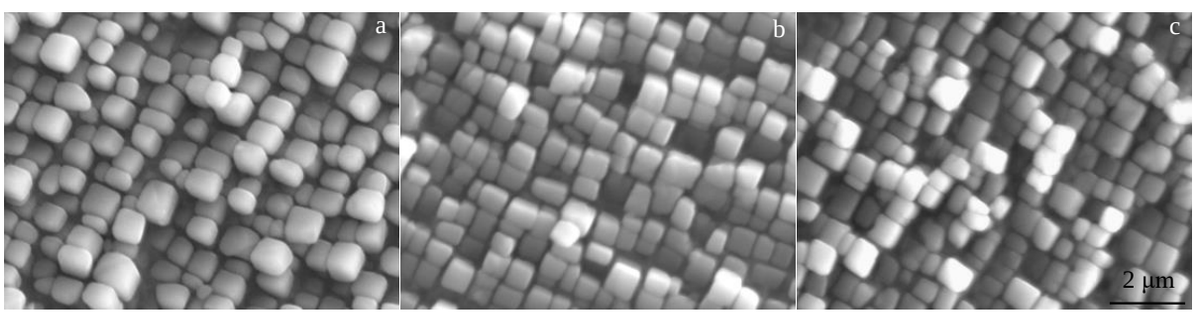

Fig.6 Morphologies of γ' phase in the dendrites with different Mn contents: (a) Mn0.09, (b) Mn0.17 and (c) Mn0.35

The stress-rupture tests were carried out at 950 °C with 235 MPa and the results are illustrated in Fig. 7. When the Mn content varies from 0.09wt% to 0.17wt%, the average rupture life changes from 55.9 h to 55.0 h, and the elongation is slightly reduced from 12.7% to 12.4%. However, when Mn content reaches 0.35wt%, the rupture life and the elongation are greatly reduced to 26.7 h and 4.1%. It seems that when Mn content is lower than 0.17wt%, it has little effect on the stress rupture properties, but when Mn content increases to a certain critical level, the stress rupture performance is greatly impaired.

The fractographs of samples with different Mn contents under stress-rupture tests are shown in Fig. 8 and all samples have a transgranular fracture manner. The facture surfaces of the three samples exhibit a dendritic morphology. Furthermore, the cross-section of Mn0.35 sample is relatively flat.

The longitudinal sections of three fractured samples tested at 950 °C with 235 MPa are shown in Fig. 9. It can be seen that cracks in all specimens are progressed along $\gamma+\gamma'$ eutectic in grain boundary and the interdendrite. The large γ' in $\gamma+\gamma'$ eutectic cap will hinder the movement of dislocations and lead to a stress concentration at the interface. Then microcrack nucleation and propagation occur[15]. So a large amount of $\gamma+\gamma'$

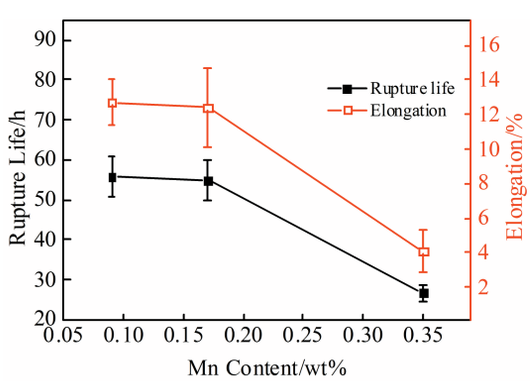

Fig.7 Effect of Mn content on the stress rupture properties of K417G at 950 °C with 235 MPa

eutectic in the grain boundary and the interdendritic region decrease the rupture life and the ductility. As shown in Fig. 9, the number of $\gamma+\gamma'$ eutectic in the margin of the fracture surface increases as the Mn content increases. This phenomenon is a good proof of the above point of view.

In nickel-base superalloy with high volume fraction of γ' phase, the distance between the γ' phases is very small, the critical stress of dislocation-cutting γ' phase is less than the

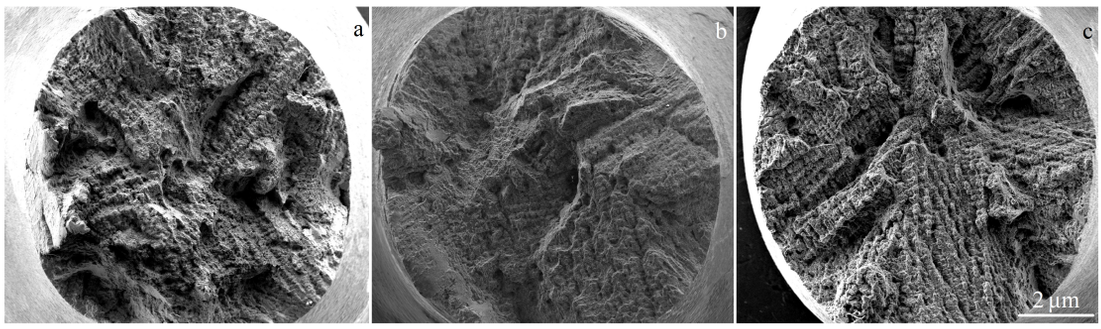

Fig.8 Full view morphologies of fracture surfaces in stress rupture test at 950 °C/235 MPa: (a) Mn0.09, (b) Mn0.17 and (c) Mn0.35

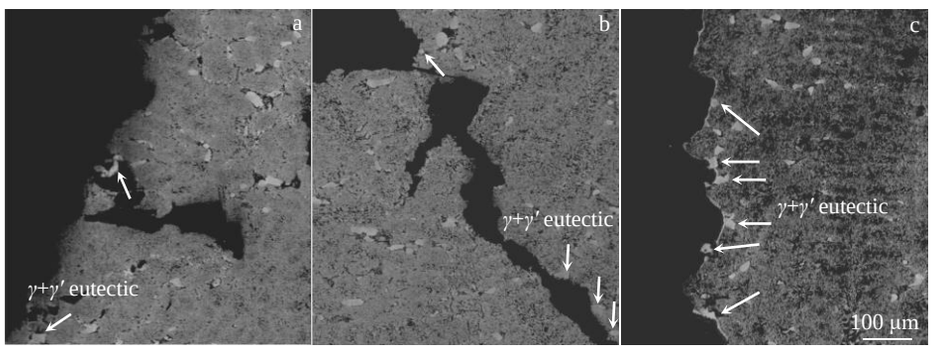

Fig.9 Fracture surfaces on the longitudinal section in stress rupture tests at 950 °C/235 MPa: (a) Mn0.09, (b) Mn0.17 and (c) Mn0.35

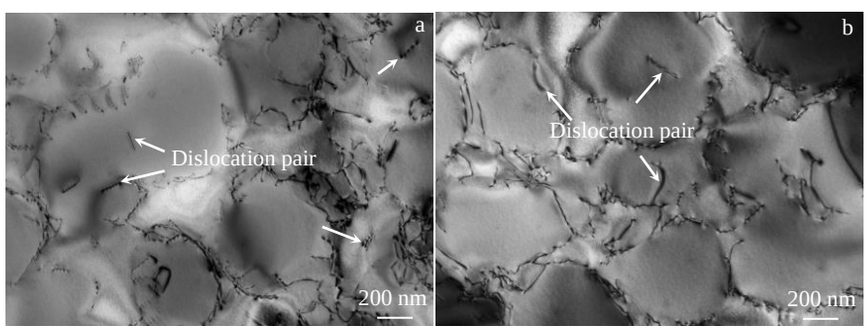

Fig.10 TEM images of dislocation structures of K417G superalloy after stress-rupture test at 950°C/235 MPa: (a) Mn0.09 and (b) Mn0.35

critical stress required for Orowan bypass mechanism, so the dislocation incising mechanism always preferentially starts[4]. In K417G alloy, the volume fraction of γ' phase is above 60%, so the dislocation cannot bypass the γ' phase, but only cut through the γ' particles. The dislocation structure after stress-rupture tests was observed through TEM and the results are shown in Fig. 10. Lots of dislocation pairs are found in γ' phase, which prove that the dislocations interact with γ' particles through APB shearing mechanism. The volume fraction of γ' phase in samples Mn0.09 and Mn0.35 is identical, but the average size of γ' phase in sample Mn0.09 is relatively large, so the width of γ matrix channel in Mn0.35 sample is smaller than that of Mn0.09 sample, namely, $d_{0.09} > d_{0.35}$. The dislocations moving within the matrix channel begin to cut γ' phase when they pile up to a certain level. The wider channel can accommodate more dislocations, and thus delay the dislocation to cut γ' phase[30]. So the rupture life of Mn0.09 sample is higher than that of Mn0.35.

3 Conclusions

1) The segregation degree of Ti, Al to the interdendritic region and Cr, Co, V, Mo to the dendrite core become obvious with the increase of Mn content in K417G alloy.

2) Mn is solid-dissolved in γ matrix. Meanwhile, Mn is slightly enriched in γ'-depleted matrix located in front of $\gamma+\gamma'$ eutectic.

3) The increase of Mn content from 0.09wt% to 0.35wt% promotes the increase of $\gamma+\gamma'$ eutectic volume fraction and the

decrease of γ' phase size.

4) The increase of Mn content in K417G alloy will deteriorate the stress rupture performance. Mn content should be controlled below 0.17wt%.

References

1 Guan Xiurong, Liu Enze, Zheng Zhi *et al*. *Journal of Materials Science & Technology*[J], 2011, 27(2): 113

2 Guo Jianting, Ranucci D, Picco E *et al*. *Metallurgical Transactions A*[J], 1983, 14(11): 2329

3 Xu Fujia, Lv Yaohui, Liu Yuxin *et al*. *Journal of Materials Science & Technology*[J], 2013, 29(5): 480

4 Guo Jianting. *Materials Science and Engineering for Superalloys* [M]. Beijing: Science Press, 2008: 184

5 High Temperature Alloy Teaching and Research Group of Beijing Iron and Steel Institute. *Superalloy Materials*[M]. Beijing: National Defense Industry Press, 1974: 217 (in Chinese)

6 Research Group of Superalloy. *Journal of Northeast University of Technology*[J], 1979, 3: 64

7 Savage W F, Krantz B M. *Welding Journal*[J], 1971, 50(7): 292

8 Morrison T J, Shira C S, Weisenberg L A. *Effect of Minor Elements on the Weldability of High Nickel Alloys*[C]. New York: Welding Research Council, 1969: 47

9 Yeniscavich W, Fox C W. *Effect of Minor Elements on the Weldability of High Nickel Alloys*[C]. New York: Welding Research Council, 1969: 24

10 Amano T, Taguchi T. *Journal of Alloys and Compounds*[J], 1993, 193(1-2): 20

11 GB/T 2039-1997[S]. 1997

12 Kearsey R M, Beddoes J C, Jaansalu K M *et al*. *Superalloys 2004*[C]. Pennsylvania: TMS, 2004: 801

13 Caldwell E C, Fela F J, Fuchs G E *et al*. *Superalloys 2004*[C], Pennsylvania: TMS, 2004: 811

14 Zhao Xinbao, Liu Lin, Yu Zhuhuan *et al*. *Journal of Materials Science*[J], 2010, 45(22): 6101

15 Gong Li, Chen Bo, Yang Yaqian *et al*. *Materials Science and Engineering A*[J], 2017, 701: 111

16 Kresse G, Furthmüller J. *Computational Materials Science*[J], 1996, 6(1): 15

17 Kresse G, Furthmüller J. *Physical Review B*[J], 1996, 54(16): 11 169

18 Blöchl P E. *Physical Review B*[J], 1994, 50(24): 17 953

19 Kresse G, Joubert D. *Physical Review B*[J], 1999, 59(3): 1758

20 Perdew J P, Burke K, Ernzerhof M. *Physical Review Letters*[J], 1996, 77(18): 3865

21 Jiang Chao, Gleeson B. *Scripta Materialia*[J], 2006, 55(5): 433

22 Jiang Chao, Sordelet D J, Gleeson B. *Acta Materialia*[J], 2006, 54(4): 1147

23 Zhu Yaoxiao, Xu Leying, Zhao Hong'en *et al*. *Acta Metallurgica Sinica*[J], 1986, 22(2): 93 (in Chinese)

24 Zhou Y Z, Volek A. *Scripta Materialia*[J], 2007, 56(6): 537

25 Miu Zhujun. *Study on Solidification Segregation and Homogenization Treatments of IN718-Type Superalloys*[D]. Shanghai: Shanghai Jiaotong University, 2011

26 Zhang Jian, Li Jinguo, Jin Tao *et al*. *Journal Materials Science & Technology*[J], 2010, 26(10): 889

27 Wang F, Ma D, Zhang J *et al*. *Journal of Crystal Growth*[J], 2014, 389: 47

28 Pyczak F, Devrient B, Neuner F C *et al*. *Acta Materialia*[J], 2005, 53(14): 3879

29 Collins D M, Heenan R K, Stone H J. *Metallurgical and Materials Transactions A*[J], 2011, 42(1): 49

30 Yu Jian, Li Jiarong, Shi Zhenxue *et al*. *Rare Metal Materials and Engineering*[J], 2013, 42(8): 1654 (in Chinese)

K417G高温合金中Mn的存在形式和分布及Mn含量对高温持久性能的影响

杨亚倩[1]，邢炜伟[1]，陈伟亮[2]，陈　波[1]，马颖澈[1]，刘　奎[1]

(1. 中国科学院金属研究所 师昌绪先进材料创新中心，辽宁 沈阳 110016)

(2. 东北大学，辽宁 沈阳 110819)

摘　要：研究了Mn含量在0.09%~0.35%（质量分数）范围内变化对K417G高温合金的高温持久性能的影响，并且探究了Mn的存在形式和分布情况。结果表明，Mn固溶于γ基体中，并偏聚于γ+γ'共晶帽前沿的γ'贫化区的基体中。Mn元素促进了Al和Ti元素向枝晶间区域的偏析，从而增加了枝晶间区域γ+γ'共晶的体积分数，减小了枝晶干中γ'相的尺寸。随着Mn含量的增加，在950 ℃/235 MPa的条件下，合金的持久寿命和塑性均大大降低。Mn含量最小的合金具有最佳的高温持久性能。

关键词：Mn含量；显微偏析；持久性能；存在形式；K417G

作者简介：杨亚倩，女，1991年生，硕士，中国科学院金属研究所，辽宁 沈阳 110016，电话：024-83970096，E-mail：yangyq@imr.ac.cn